AJVR

AVMA

^{18}F-sodium fluoride positron emission tomography is a sensitive imaging technique to detect atherosclerosis in Amazon parrots (*Amazona* spp)

Lucyanne Megan, DVM[1]; Kelsey Brust, DVM, DACVR[2]; Matthieu Spriet, DVM, MS, DACVR, DECVDI, DACVR-EDI[2]; Pedro Ruivo, DVM, MS, DACVP[3]; Marcel Gómez-Ponce, DVM[4]; Hugues Beaufrère, DVM, PhD, DACZM, DABVP (Avian), DECZM (Avian)[1,4]*

[1]Department of Medicine and Epidemiology, School of Veterinary Medicine, University of California-Davis, Davis, CA
[2]Department of Surgical and Radiological Sciences, School of Veterinary Medicine, University of California-Davis, Davis, CA
[3]Comparative Pathology Laboratory, School of Veterinary Medicine, University of California-Davis, Davis, CA
[4]Graduate Group in Integrative Pathobiology, School of Veterinary Medicine, University of California-Davis, Davis, CA

*Corresponding author: Dr. Beaufrère (hbeaufrere@ucdavis.edu)

OBJECTIVE
To investigate and establish a protocol for ^{18}F-sodium fluoride (^{18}F-NaF) PET scan imaging in Amazon parrots for atherosclerosis diagnosis.

METHODS
In this feasibility proof-of-concept study, ^{18}F-NaF µPET scan and µCT scan were obtained on Hispaniolan (*Amazona ventralis*) and orange-winged Amazon parrots (*A amazonica*). A different µPET scan protocol was used for each species. Images were reviewed by 3 observers for arterial calcification and radiotracer uptake indicative of atherosclerosis. A blood lipid profile was also performed. A subset of Hispaniolan Amazon parrots were euthanized after completion of the study, and the heart and arteries were collected for histopathology.

RESULTS
10 adult Hispaniolan and 8 adult orange-winged Amazon parrots were scanned. Atherosclerotic lesions were detected on both µCT and µPET scan in various arteries. The presence of streak artifacts and increased noise on µCT scan limited the ability to detect high-attenuation areas of arteries and obtain observer consensus except for 1 case of severe arterial calcification. µPET scan was overall more sensitive, had higher interobserver agreement in lesion scoring, and detected a higher number of lesions in both species, including in coronary arteries. On histopathology on 5 Amazon parrots, the majority (5/6) of clinically relevant atherosclerotic lesions and some preatheromatous lesions (1/3) were identified on µPET scan. No association between atherosclerosis detection on µPET scan and the lipid profile was observed.

CONCLUSIONS
This study established a safe and effective protocol for ^{18}F-NaF molecular imaging of psittacine atherosclerosis, which proved to be more sensitive than CT scan.

CLINICAL RELEVANCE
^{18}F-sodium fluoride PET scan allows for a more reliable and earlier diagnosis of atherosclerotic lesions in Amazon parrots.

Keywords: atherosclerosis, arteriosclerosis, Psittaciformes, PET scan, sodium fluoride

Atherosclerosis is a common arterial lesion in a wide range of avian species, particularly in Psittaciformes.[1] The background prevalence of clinically relevant atherosclerotic lesions (moderate-to-severe lesions) in companion psittacine birds has been estimated at 7%, but the prevalence is affected by sex, age, species, and comorbid conditions.[2] For instance, it can be as high as 50% in geriatric female birds of predisposed species, such as Amazon parrots (*Amazona* spp) and grey parrots (*Psittacus erithacus*).[2]

As in mammals, atherosclerotic lesions are inflammatory lesions characterized in birds by the

Received October 14, 2024
Accepted November 6, 2024
Published online December 2, 2024

doi.org/10.2460/ajvr.24.10.0303

© 2025 THE AUTHORS. Published by the American Veterinary Medical Association as an Open Access article under Creative Commons CCBY-NC license.

Unauthenticated | Downloaded 04/19/25 06:02 AM UTC

accumulation of macrophages, cholesterol, other lipids, and necrotic debris in the intima and the luminal side of the media of arteries, and lesions can be calcified and fibrotic.[3] Lesions are reported to be more common in the central arteries at the base of the heart in parrots, such as the aorta, the brachiocephalic trunks, and the pulmonary arteries, but can also be found in coronary and peripheral arteries.

The diagnosis of atherosclerosis is challenging in psittacine birds antemortem. While dyslipidemic changes have been associated with the lesions and various lipidologic tests have been investigated in parrots in relation to lipid-accumulation disorders,[4–8] they only assess risk factors and do not help in detecting, staging, and monitoring lesions in arteries. The lesions must be identified on vascular imaging techniques. However, current imaging techniques are insensitive to diagnose all but the most advanced lesions because of a combination of factors, such as the small size of psittacine birds, the extremely fast heart rate, the presence of air sacs surrounding the heart, and the presence of a large keel bone shielding the heart ventrally and laterally. Echocardiography is seldom useful to detect atherosclerotic lesions of the great arteries in relation to other cardiac abnormalities. Two strategies have been used to attempt to image these lesions: detecting luminal stenosis by angiography or detecting arterial calcification.

Since arterial luminal stenosis is the main pathophysiological mechanism involved in psittacine atherosclerotic diseases, angiographic protocols were developed in parrots, including CT angiography and fluoroscopic angiography.[9–13] However, the arterial luminal diameters of medium-sized parrots are only 1.5 to 3 mm, and significant motion artifacts are present at the base of the heart, which makes angiography poorly sensitive except for severe stenosis. The clinical use of angiography to detect atherosclerotic arterial luminal stenosis has not been reported in parrots so far and would require method-specific reference intervals for arterial luminal diameters in multiple species of parrots. Therefore, clinical angiographic protocols will likely remain extremely limited by both technical and practical considerations in the future while not directly diagnosing atherosclerosis.

Arterial calcification is a hallmark of atherosclerosis in mammals and birds and ranges from microcalcification to complete bone tissue formation.[3,14,15] In mammals, coronary calcification is an active process resembling osteogenesis, is triggered by the inflammatory process of plaque formation and cell apoptosis, and is regulated by complex enzymatic and cellular pathways.[15] The biological significance of arterial calcification is unknown, but the amount of calcification is associated with the progression of atherosclerosis and biomechanical changes to the atheromatous plaques.[15] In parrots, arterial calcification is also strongly associated with advanced and clinically significant lesions (types IV to VII histologic lesions, characterized as atheromas or fibroatheromas on the psittacine classification scheme) and is correlated to lesion area, but microcalcification can be seen in earlier lesions.[3] Arterial calcification is also present in diet-induced atherosclerotic lesions in experimental parrot models and can be detected as early as 4 months on an increased cholesterol diet.[5] Since arterial calcification is highly specific for atherosclerosis, it can be used as a surrogate imaging marker of atherosclerotic lesion burden. Radiography and CT imaging can be used to detect arterial calcification. A computed tomography scan is more sensitive for the detection of arterial calcium and allows measurement of both the density and extent of arterial calcification.[16] In people, a coronary calcium score has been widely used for staging coronary arterial disease and to predict future acute coronary events.[17] Arterial calcification is cumulative and associated with the progression and severity of atherosclerotic lesions, but only macrocalcifications over a 200-µm diameter, associated with more severe and irreversible lesions, can be detected on clinical CT scans, which typically have a 0.4- to 0.6-mm resolution.[18] Microcalcifications (defined as areas under 50 µm) are not detectable using clinical CT scans.[19] From our experience, while cases with advanced lesions and severe calcification can be diagnosed on CT scan, a CT scan still seems poorly sensitive overall for the diagnosis of psittacine atherosclerosis when correlating to necropsy findings.

As arterial calcification is strongly associated with atherosclerotic lesions in parrots, imaging techniques with increased sensitivity would be ideal to diagnose earlier reversible lesions of atherosclerosis in captive psittacine birds. This would allow earlier medical intervention at a stage where lesions may still be reversible or not progress to clinically significant lesions with appropriate management of risk factors. It would also allow better screening and monitoring of lesions and be applicable to further research on the pathophysiology, understanding of plasma lipid risk factors, and treatment of this common condition of captive and companion parrots.

Molecular imaging using PET scanners has been used in people and in laboratory animals for diagnosing atherosclerotic lesions. While structural imaging, such as a CT scan, is limited to macroscopic changes arising in late stages of atherosclerotic plaque formation, molecular imaging can visualize early stages of the disease, microscopic changes, and various intraplaque metabolic or dynamic processes.[20] Despite a lower spatial resolution than CT scans, the affinity of radiotracers for particular compounds allows the visualization of inflammation, apoptosis, and early calcification.[16,20] In particular, ^{18}F-sodium fluoride (^{18}F-NaF) is a marker of microcalcification that has been extensively used in the diagnosis of early atherosclerosis in people over the past 10 years but not yet used in veterinary medicine for this purpose. ^{18}F-sodium fluoride, once injected IV, exchanges with hydroxyl groups on exposed regions of hydroxyapatite crystals on the surface of calcified areas (bones and arterial calcification) to form fluoroapatite.[18] It has a radioactive half-life of 110 minutes and decays by positron emission. The tracer uptake is mainly

Unauthenticated | Downloaded 04/19/25 06:02 AM UTC

dependent on blood flow and the surface area of exposed hydroxyapatite. For this reason, uptake may be higher in extensive microcalcified areas than in large macroscopic deposits, and an ^{18}F-NaF PET scan reflects the surface area of microcalcification rather than tissue density like in CT scan images.

^{18}F-sodium fluoride molecular imaging of psittacine atherosclerotic lesions has not been attempted before and would bypass the many limitations of conventional imaging of these lesions as well as considerably increase diagnostic sensitivity, which could be a game changer in the early diagnosis of this disease in birds. The objectives of this feasibility proof-of-concept study were to investigate and establish a protocol for ^{18}F-NaF PET scan imaging in parrots using Amazon parrots, species highly prone to atherosclerosis, from 2 research colonies maintained at the University of California (UC)-Davis, 1 of which includes birds that have been hypercholesterolemic for years. We hypothesize that the ^{18}F-NaF PET scan would be a highly sensitive imaging technique to detect arterial lesions consistent with atherosclerosis in Amazon parrots.

Methods

An IACUC was approved for this study by UC-Davis (#23181).

Animals

Two species of Amazon parrots from the UC-Davis psittacine research colonies were used for this research: 10 Hispaniolan Amazon parrots (HAPs) (*A ventralis*) with a median (range) age of 20 (18 to 34) years and a mean ± SD weight of 294 ± 21 g, comprised of 4 females and 6 males, and 8 orange-winged Amazon parrots (*A amazonica*) (OWAPs) with a median (range) age of 42.5 (34 to 50) years and a mean ± SD weight of 375 ± 43 g, comprised of 2 females and 6 males. To increase the likelihood of selecting birds with atherosclerotic lesions, older individuals were chosen from the colonies. In addition, the HAP colony had a history of chronic hypercholesterolemia that was first evidenced about 10 years prior to the study.[21]

The sample size selected for the study was based on prevalence estimates of clinically significant lesions in older Amazon parrots[2] in order to have a minimum number of cases with advanced atherosclerosis and, likely, other cases with milder lesions. It was also thought that this sample size would allow the presence of a variety of lesion severity, vascular distribution, and lesion calcium content in both micro- and macrocalcified atherosclerotic lesions.

Five out of the 10 HAPs were euthanized several weeks after completion of the study due to unrelated conditions that were diagnosed on imaging, such as advanced arthritis. Decisions were also based on low quality-of-life scores and feedback from the UC-Davis IACUC. These birds were euthanized by IV administration of potassium chloride under isoflurane anesthesia.

Imaging

Birds were transported to the UC-Davis Center for Molecular and Genomic Imaging. Each bird was sedated with midazolam (3 mg/kg, IM) and butorphanol (3 mg/kg, IM). One mL of blood was collected from the right jugular vein and transferred to EDTA tubes (Microtainer; BD).

A 26-gauge IV catheter was placed in the ulnar vein. A dose of 18.5 MBq (0.5 mCi) of ^{18}F-NaF was administered IV using a shielded syringe followed by a 0.2- to 0.5-mL 0.9% NaCl flush. The injected dose was verified by pre- and postinjection radioactivity measurements of the syringe using a dose calibrator. The IV catheter was then removed, and the bird was placed back in its carrier.

For HAPs, a 60-minute waiting period was implemented between injection time and imaging time. Because of perceived high residual background activity in blood in the HAPs, the waiting period was extended to 120 minutes in OWAPs.

Birds were then administered an additional 1 mg/kg of midazolam, IM, and maintained on 100% oxygen and 0.5% to 1% isoflurane via a facemask during scanning, and respiratory rate was monitored visually. The parrots were imaged using a combined µCT/µPET scanner (GNEXT PET/CT; Sofie) with automatic colocalization. The µPET images were acquired for 20 minutes as static acquisition with a PET resolution of < 1 mm. The µCT resolution was 75 µm and was a cone-beam CT scan (CBCT). Only the caudal body was imaged, excluding the head and cranial neck.

Once image acquisition was completed, the parrots were recovered, and an injection of flumazenil (0.1 mg/kg, IM) was administered in addition to SC fluids at 20 mL/kg. Following recovery, the birds were transferred to a radiation isolation room at the UC-Davis Veterinary Medical Teaching Hospital until the following morning. The radiation level was measured at the surface of the birds using a Geiger counter to ensure that it was below the radiation safety release threshold (< 2 mrem/h) prior to returning them back to the colony.

In addition, for the 5 euthanized HAPs, a post mortem multidetector CT (MDCT) scan was performed within 1 hour using a GE LighSpeed16 (GE HealthCare) with a slice thickness of 0.625 mm.

Image analysis and interpretation

Images were imported into an open-source imaging software (3D slicer, version 5.0.3; https://www.slicer.org).[22] Micro-Positron Emission Tomography (µPET) images were fused with the µCT images for interpretation.

Images were first analyzed qualitatively by assessing different arterial segments of interest, including brachiocephalic trunks, ascending aorta, descending aorta, and pulmonary arteries, by 3 different observers (1 diagnostic imaging specialist, 1 zoological medicine specialist, and 1 zoological medicine resident). Other smaller arteries were also assessed depending on ease of visualization and

Unauthenticated | Downloaded 04/19/25 06:02 AM UTC

included the celiac artery, the cranial mesenteric artery, the iliac arteries, the coronary arteries, the subclavian arteries, and the carotid arteries. General tracer uptake was also reported as it may affect interpretation of the vascular system.

Computed tomography images were evaluated for the presence of abnormal sites of arterial calcification that were readily visible on a 0 to 2 score, with 0 being no calcification, 1 being mild calcification, and 2 being moderate-to-severe calcification. Positron emission tomography images were adjusted to a threshold that minimized background activity visualization, using the pectoral muscles and/or caudal vena cava as reference points (standardized uptake value [SUV] window level approx varying between 10 and 20 and SUV window width varying between 20 and 30 depending on studies and acquisition protocols). Arterial tracer uptake was then assessed and semiquantitatively scored from 0 to 2, with 0 being no uptake, 1 mild uptake, and 2 moderate-to-high uptake. Colocalization of lesions between imaging techniques was also recorded qualitatively.

Several analytical values were then obtained using the imaging software by 1 observer (HB). Each artery was segmented manually in regions of interest (ROI) using the "segment editor" module. The brachiocephalic trunks were segmented from their emergence from the ascending aorta or base of the heart to the branching of the subclavian arteries, the ascending aorta was included from its bifurcation from the right brachiocephalic trunk to its position immediately dorsal to the heart, the descending aorta was segmented from the celiac artery to the cranial division of the kidney, and the pulmonary arteries were included from their emergence from the heart to the beginning of the pulmonary parenchyma. In addition, areas of the caudal vena cava, right liver lobe, and pectoral muscles were obtained to measure background tracer uptake.

For µPET scan images, areas of spill-in effects from adjacent boney areas of high tracer uptake (keel, coracoids, syrinx, primary bronchi) were excluded as much as possible.[23] Then, the mean SUV (SUV_{mean}) and maximum SUV (SUV_{max})[20] as well as the segmented arterial volumes (in mm^3) were obtained. Other variables were then calculated and included the background corrected SUV_{max} ($SUV_{max} - SUV_{mean\ of\ caudal\ vena\ cava}$), the mean and maximum target-to-background ratios (TBR; $TBR_{mean} = SUV_{mean}/SUV_{mean\ of\ caudal\ vena\ cava}$ and $TBR_{max} = SUV_{max}/SUV_{mean\ of\ caudal\ vena\ cava}$), and the volumetric percentage of segmented arteries above TBR = 1.5.[20] The caudal vena cava values were used for background correction.

For µCT scan and MDCT images, segmented ROIs were thresholded to only include pixels above an attenuation of 130 Hounsfield units (HU) to obtain calcium score data.[17] The µCT scan, being a CBCT, did not inherently display attenuation values in HU and was calibrated by the manufacturer to obtain HU-equivalent values from grey values. Volume and mean HU of the thresholded ROIs were obtained and used to calculate the relative calcium mass score (volume X mean HU/100).[24]

Lipoprotein analysis

Advanced lipoprotein profiling was performed on EDTA plasma using a high-resolution PAGE kit (LDL Lipoprint Kit; Quantimetrix) according to the manufacturer instructions. The lipoprotein profile included very-low-density lipoprotein cholesterol, intermediate-density lipoprotein cholesterol, low-density lipoprotein cholesterol, and high-density lipoprotein (HDL) cholesterol relative and absolute concentrations. Calculated values were also obtained and included non–HDL cholesterol and HDL/total cholesterol ratio. Total cholesterol and triglycerides were obtained using a dedicated benchtop analyzer (Cholestech LDX; Abbott Laboratories).

Histopathology

The heart and arteries were collected from the 5 euthanized HAPs. Cross-sections of arteries (brachiocephalic trunks, pulmonary arteries, ascending aorta, abdominal aorta) were obtained at the sites of maximum radiotracer uptake and maximum HU values whenever applicable. For arteries with minimum radiotracer uptake, general sections of the arteries were obtained. The heart was sectioned at its base at the level of the coronary sulcus and midventricular to assess the origins of the main arteries as well as the coronary arteries. Tissue sections were routinely processed for histopathology using H&E stain and von Kossa stain for calcium. Slides were reviewed by a board-certified veterinary pathologist, and atherosclerotic lesions were graded according to a published classification system in psittacine birds.[3]

Statistical analysis

Most data were analyzed descriptively and reported with median (range). Linear mixed models were used to assess the association between sex, species/protocol (HAPs at 1 hour or OWAPs at 2 hours), arteries (brachiocephalic trunks, pulmonary arteries, ascending and abdominal aorta), blood lipids, and imaging measurements. Individual parrots were used as the random effect. Assumptions of linearity, homogeneity or variances, and normality were assessed on residual plots and quantile plots. If model assumptions were not met, outcome variables (imaging measurements) were log transformed, and assumptions were rechecked. An ANOVA was performed on fixed effects, and a Tukey adjustment was used for post hoc analysis.

Wilcoxon rank-sum tests were performed between protocols to look at the effect of waiting time prior to scanning on organ background SUV_{mean} values.

R (version 4.4.1; R Foundation for Statistical Computing) was used for statistical analysis, and an alpha of 0.05 was used for statistical significance.

Results

There was no morbidity or mortality during the course of this study and after image acquisition.

Unauthenticated | Downloaded 04/19/25 06:02 AM UTC

General tracer uptake distribution

As anticipated for ^{18}F-NaF, there was pronounced uptake observed throughout the bones and articulations, with less uptake in pneumatized bones overall. This extended to calcified cartilaginous structures, such as the tracheal and bronchial rings, with noticeably more uptake in the tracheal and bronchial syringeal cartilages. There was marked interindividual variation in the skeletal distribution of tracer uptake. In particular, arthritic joints were associated with intense radiotracer uptake in some birds, which was readily observed in appendicular articulations but also in the neck and at the notarium-synsacrum free vertebra junction. In females, all medullary bones, including appendicular bones and all vertebrae, had profound radiotracer uptake, which was interpreted as a polyostotic hyperostosis process due to estrogen stimulation.

Several structures interfered with the assessment and measurement of radiotracer activity in the arteries because of the spill-in effect of closely associated calcified structures. Specifically, the coraco-sternal articulation activity spilled in the adjacent brachiocephalic trunks on their ventral aspects, and the bronchial syringeal cartilages spilled in the adjacent pulmonary arteries on their medial aspects **(Figure 1)**. This was expected to lead to substantial overestimation of SUV values despite excluding these areas in the ROIs.

Sodium fluoride is excreted in the urine,[25] and, consequently, uptake was very high in the kidneys and the cloaca. Uptake was also high in the rectum and distal colon, particularly in 2-hour-delay studies, due to physiologic urine backflow in the distal gastrointestinal system and retrograde peristalsis. Activity in the kidneys and distal colon interfered with interpretation of uptake in the distal abdominal aorta and its branches. Observed hepatic and caudal vena cava uptake were considered to be higher than what would be expected for background activity, especially considering that NaF is rapidly eliminated from the blood stream, with as little as 10% left 1 hour after administration in people.[25] This was attributed to the reabsorption of NaF in the colon, resulting from the retrograde peristalsis of urine. This was supported by the fact that the SUV_{mean} of pectoral muscles was not significantly different between the 1-hour and the 2-hour protocol (P = .33), whereas the SUV_{mean} of the liver and caudal vena cava were significantly higher at 2 hours (P = .027 and P = .006, respectively).

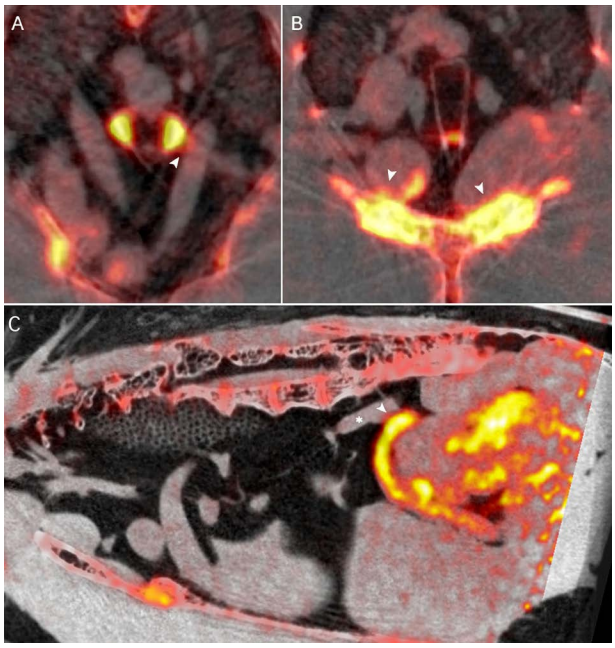

Figure 1—Fused µCT/µPET images illustrating spill-in effects of adjacent mineralized structures. A—Tracheal syringeal cartilages with spill-in effect in adjacent right pulmonary artery (white arrowhead). B—Spill-in effect of coracosternal joints in adjacent ventral brachiocephalic trunks bilaterally (white arrowheads). Atherosclerotic lesions are also seen in the brachiocephalic trunks, and streak µCT artifacts are visible. C—Sagittal view of an orange-winged Amazon parrot (left is cranial) showing the spill-in effect of radiotracer in the rectum (white arrowhead) to the abdominal aorta (asterisk) with image acquisition 2 hours after radiotracer administration. The large amount of activity caudally is the cloaca.

Lesion detection and distribution

Atherosclerotic lesions were detected on both the µCT and µPET. The distribution of lesions among arteries is reported in **Table 1**.

Table 1—Atherosclerotic lesion detection in 2 cohorts of Amazon parrots (*Amazona* spp) by calcification graded on µCT scan and ^{18}F-sodium fluoride uptake graded on µPET scan.

				µCT grade			µPET grade		
Species	**Protocol**	**N**	**Arteries**	**0**	**1**	**2**	**0**	**1**	**2**
HAP	1 hour	10	Brachiocephalic trunks	7	3	0	6	1	3
			Ascending aorta	10	0	0	8	2	0
			Abdominal aorta	5	4	1	8	1	1
			Pulmonary trunks	8	2	0	8	2	0
			Coronary arteries	10	0	0	9	1	0
OWAP	2 hours	8	Brachiocephalic trunks	8	0	0	3	2	3
			Ascending aorta	8	0	0	4	3	1
			Abdominal aorta	7	0	1	3	4	1
			Pulmonary trunks	7	0	1	5	3	0
			Coronary arteries	8	0	0	2	4	2

HAP = Hispaniolan Amazon parrot. OWAP = Orange-winged Amazon parrot.

Unauthenticated | Downloaded 04/19/25 06:02 AM UTC

Lesions were detected on µCT scan in 7 out of 10 HAPs and 1 out 8 OWAPs (Table 1). However, only 1 bird, an HAP with an advanced calcified lesion of the abdominal aorta, had a consensus among the 3 observers. The large amount of noise and streak artifacts associated with CBCT imaging[26] rendered the assessment of high-attenuation areas difficult on the arteries, especially for HAPs as they were smaller than OWAPs by about a third. The brachiocephalic trunks were also more affected by streak artifacts being adjacent to the keel and coracoids (Figure 1) and the ascending aorta evaluation more impacted by noise due to its smaller size. On standard MDCT scans performed on the 5 euthanized HAPs, only the advanced calcified lesion in the aorta of 1 bird was detected. No calcification in the areas of coronary arteries or ascending aorta was detected on either CT modality.

On µPET scan, lesions were seen in 4 out of 10 HAPs and 7 out of 8 OWAPs (**Figure 2**; Table 1). A consensus on the presence of lesions on µPET scan was reached in 9 out of 11 of these birds and in all lesions with moderate-to-severe radiotracer uptake. Intracardiac radiotracer uptake estimated to be near the coronary groove area and interventricular septum was seen in 1 HAP and 6 OWAPs. This pattern of uptake, particularly when it followed a linear or tracing pattern, was interpreted as indicative of coronary lesions (Figure 2). Most birds had lesions in more than 1 artery. Overall, when lesions were present, they were not uniformly distributed throughout the arterial walls, with certain areas having generally higher radiotracer uptake depending on the artery. For the brachiocephalic trunks, while lesions were seen at various locations, the base and the bifurcation with the subclavian arteries tended to have more prominent radiotracer uptake when positive. For the abdominal aorta, lesions were most often located at the bifurcation with the celiac artery but could be seen at various other locations. Lesions generally did not colocalize well with the lesions suspected on µCT. For the bird with the highly calcified lesion seen in the abdominal aorta on µCT and MDCT, only mild radiotracer uptake was seen on the µPET scan **(Figure 3)**.

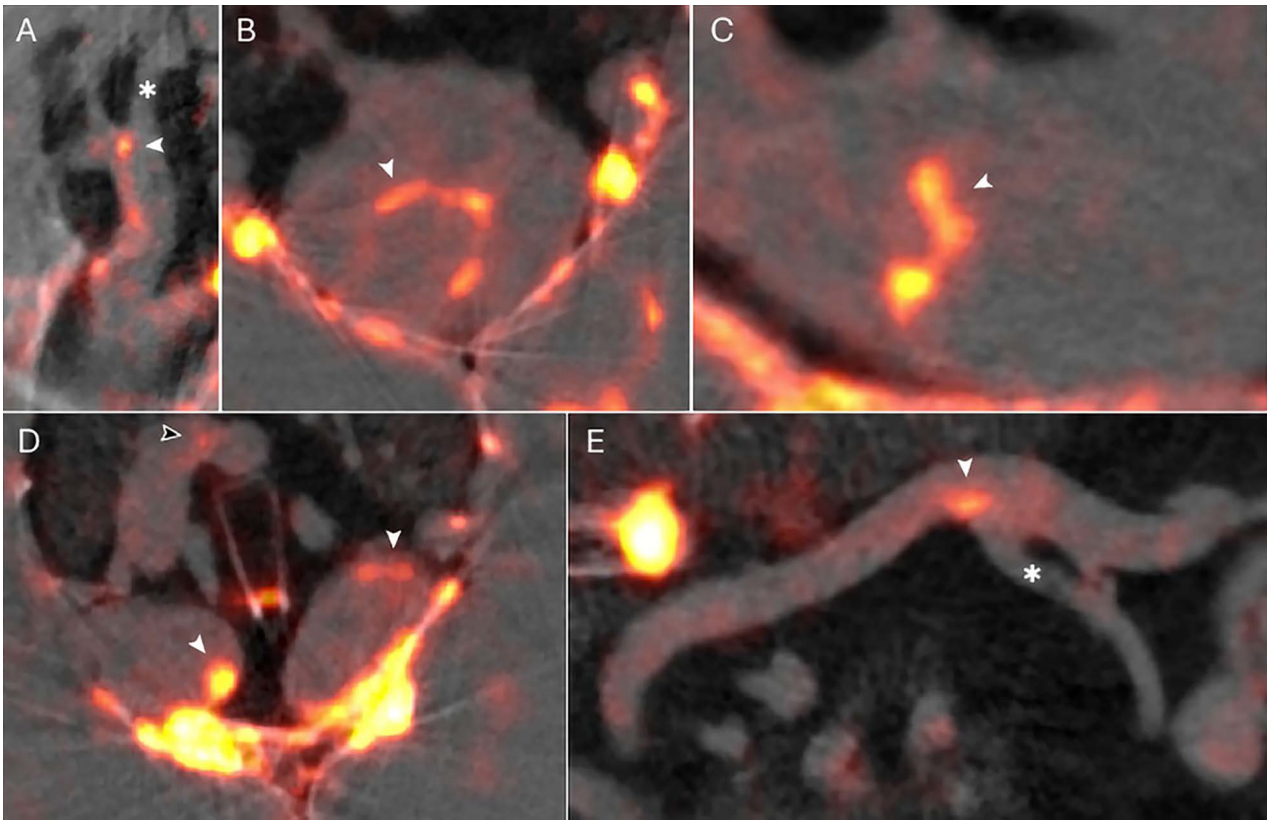

Figure 2—Moderate-to-severe NaF uptake in atherosclerotic lesions identified in Amazon parrots (*Amazona* spp) on µPET scan. Fused µCT/µPET images in various orientations. A—Longitudinal section obtained by multiplanar reconstruction of the right brachiocephalic trunk from its emergence to the subclavian artery bifurcation (bottom, ventral; left, lateral). Patchy radiotracer uptake is seen along the lateral arterial wall with more pronounced uptake (white arrowhead) near the bifurcation with the subclavian artery and carotid artery (asterisk). B—Axial and (C) sagittal views of the heart showing radiotracer uptake along coronary arteries (white arrowheads). D—Cross-sectional image at the level of the brachiocephalic trunk with marked radiotracer uptake (white arrowheads); less pronounced uptake is also seen in the ascending aorta (black arrowhead). E—Longitudinal section obtained by multiplanar reconstruction of the abdominal aorta (left is cranial) exhibiting radiotracer uptake (white arrowhead) at the bifurcation with the celiac artery (asterisk).

Unauthenticated | Downloaded 04/19/25 06:02 AM UTC

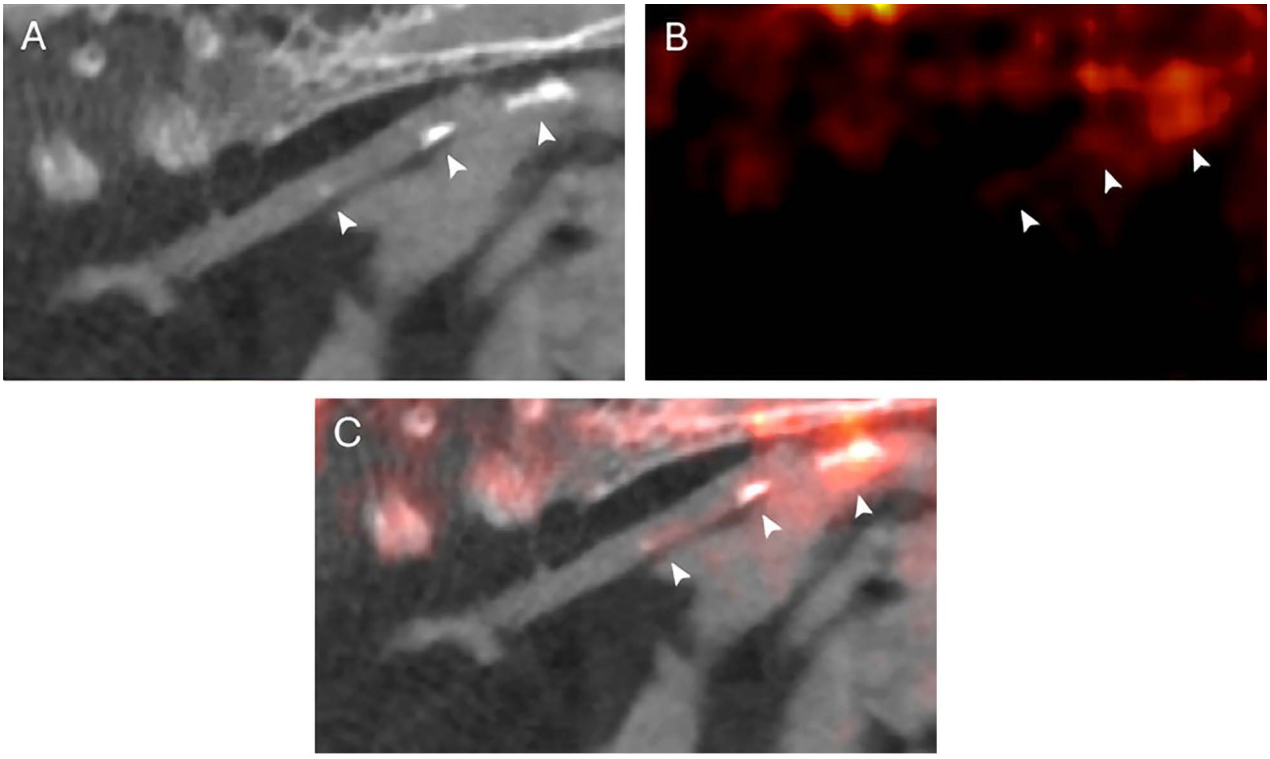

Figure 3—Sagital section at the level of the abdominal aorta in a Hispaniolan Amazon parrot illustrating minimal radiotracer uptake in macrocalcific lesions (left is cranial). A—Micro computed tomography (μCT) scan image. B—Micro positron emission tomography (μPET) scan image. C—Fused μCT/μPET scan image. White arrowheads indicate macrocalcific lesions in abdominal aorta.

Sensitivity based on histopathology

All 5 euthanized HAPs had lesions diagnosed on histopathology of the arteries. Lesion types on the main arteries included 4 arteries with type V lesions (3 brachiocephalic and 1 ascending aorta), 2 with type IV lesions (1 abdominal and 1 ascending aorta), 3 with type III lesions (all abdominal aorta), 3 with type II lesions (1 ascending, 1 abdominal aorta, and 1 brachiocephalic), and 7 with type I lesions (4 pulmonary arteries, 1 brachiocephalic, and 2 ascending aorta). All clinically relevant lesions (types IV through VI) except 1 were detected on the μPET scan, whereas only 1 (the advanced calcified lesion in abdominal aorta) was detected on the MDCT scan and convincedly on the μCT scan (at least 2 observers agreed) **(Figure 4)**. One intermediate lesion (type III) out of 3 was detected on the μPET scan. Some preatheromatous lesions (types I and II) were also detected, but detection rate and interobserver consensus were low for these lesions. Regarding the coronary arteries, all birds exhibited coronary lesions on histopathology, but only 1 had an advanced lesion, a type V. The lesion in this bird was positive on the μPET scan, whereas the other 4 birds were negative. Most advanced lesions had calcification detectable on the von Kossa stain.

Imaging values

Values measured on different lesions identified on μPET scan images are reported in **Table 2**. Due to the presence of artifacts impacting the ability to obtain accurate and representative imaging values on the μCT and the low agreement between observers, μCT-scan values were not reported.

A significant interaction effect between protocol and arteries was seen for SUV_{max} (P = .031). On post hoc analysis, SUV_{max} was significantly higher in the OWAP/2-hour protocol when compared to the HAP/1-hour protocol for all arteries (all P < .05). Within both species, the brachiocephalic trunks had significantly higher SUV_{max} than all other arteries (all P < .05). The background corrected SUV_{max} showed analogous results.

The mean SUV was log transformed to meet model assumptions. Mean SUV was significantly higher in the OWAP/2-hour protocol than in the HAP/1-hour protocol (P = .002) and also in the brachiocephalic trunks when compared to other arteries (all P < .05).

For TBR_{mean}, significant differences were only observed between arteries (P < .001) but not between protocols (P = .57). The brachiocephalic arteries had higher TBR_{mean} than other measured arteries (all P < .001). Values for TBR_{max} and percentage of TBR > 1.5 were log transformed to meet model assumptions, but showed similar findings with significant differences only observed between arteries (P < .001) with the brachiocephalic trunks having higher values than other arteries (all P < .001).

Sex did not have an effect on any μPET scan measurements (all P > .05).

Unauthenticated | Downloaded 04/19/25 06:02 AM UTC

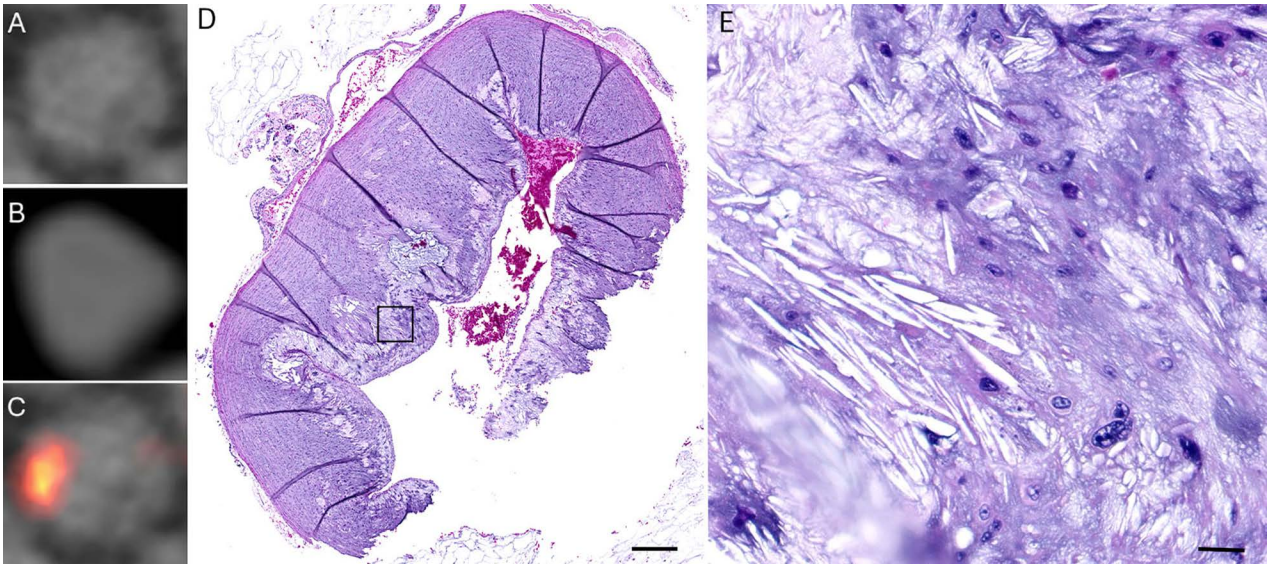

Figure 4—Cross-sections at the same level of the right brachiocephalic trunk in a Hispaniolan Amazon parrot using µCT scan (A), MDCT scan (B), µPET scan (C), and histopathology (D; H&E stain; scale bar = 400 µm). Atherosclerosis is not detected on CT scan images but showed strong radiotracer uptake on the wall in µPET scan images. Histopathology confirmed the presence of an atherosclerotic type IV lesion at that location. E—Magnification of the lipidonecrotic core (square area from [D]) showing cholesterol cleft, extracellular fat, and cellular debris (H&E stain; scale bar = 20 µm).

Table 2—^{18}F-sodium fluoride/µPET scan values in 2 cohorts of Amazon parrots (*Amazona* spp) grouped by lesion grades.

Species	Protocol	µPET scan grade	N	SUV_{max} (median, range)	SUV_{mean} (median, range)	TBR_{max} (median, range)	TBR_{mean} (median, range)	Percentage of TBR > 1.5 (median, range)
HAP	1 hour	0	30	1.4 (0.8–2.6)	0.9 (0.6–1.3)	2.0 (1.2–4.0)	1.0 (0.8–1.6)	9 (0–53)
		1	6	2.3 (1.8–2.6)	1.3 (1.2–1.4)	2.0 (1.6–2.7)	1.0 (0.9–1.3)	5 (0–32)
		2	4	3.2 (2.4–3.9)	1.6 (1.5–1.7)	2.6 (2.1–3.4)	1.3 (1.0–1.5)	24 (14–39)
OWAP	1 hour	0	15	2.7 (2.0–6.0)	1.4 (1.2–2.8)	2.2 (1.1–2.9)	1.1 (0.6–1.4)	11 (0–33)
		1	12	4.1 (3.1–7.1)	2.5 (1.7–3.6)	2.1 (1.4–3.3)	1.2 (1.0–1.4)	15 (0–45)
		2	5	5.8 (4.9–8.4)	2.5 (1.2–3.6)	2.7 (2.3–6.0)	1.2 (1.0–1.3)	14 (4–22)

HAP = Hispaniolan Amazon parrot. OWAP = Orange-winged Amazon parrot. SUV = Standardized uptake value. TBR = Target-to-background ratio using caudal vena cava as the background.

Association with blood lipids

No association was detected between imaging values and blood cholesterol, triglycerides, and lipoproteins (all $P > .05$).

Discussion

This study demonstrated that µPET scanning is a safe and effective imaging technique for the detection of atherosclerotic lesions in Amazon parrots. Micro Positron Emission Tomography scan showed much higher sensitivity in detecting atherosclerotic lesions compared to µCT scan or MDCT scan in this cohort. For parrots whose histopathologic data were available, the majority (5/6) of clinically relevant atherosclerotic lesions were identified on µPET scan compared to minimal detection (1/6) on CT modalities. Additionally, intermediate lesions were only detectable on µPET scan (1/3). This is similar to what is seen in humans, where a PET scan is used to identify earlier-stage lesions compared to the later-stage, frequently irreversible lesions seen on CT scan.[20] The low detection rate of atherosclerotic lesions on CT scan in Amazon parrots has clinical implications on clinical management as diagnosis of atherosclerosis may be frequently missed with this modality.

Some atherosclerotic lesions were detected in the large arterial trunks at the base of the heart or the abdominal artery on µPET and µCT imaging modalities, whereas lesions in the coronary arteries were only appreciated on µPET scan. This suggests that a PET scan is uniquely able to detect atherosclerotic lesions in smaller arteries in psittacine birds. In psittacines, atherosclerotic lesions have been most commonly reported in the great arteries at the base of the heart, with lesions in the abdominal aorta, coronary arteries, and other peripheral arteries less frequently documented.[1] However, across imaging modalities in our study we identified lesions in the abdominal aorta in 10 of 18 (55.5%) birds evaluated

Unauthenticated | Downloaded 04/19/25 06:02 AM UTC

and coronary lesions in 7 of 18 (38.9%) birds. This discrepancy may be due to underdiagnosis of atherosclerotic lesions in peripheral vessels on necropsy due to a lack of sampling at these sites. Our findings underscore the importance of thoroughly evaluating arteries beyond the central ones in birds submitted for histopathology with suspected atherosclerosis, with particular attention to the coronary arteries and the abdominal aorta. Micro Positron Emission Tomography scan values were consistently higher for the brachiocephalic trunks than for other arteries. While lesions were frequently detected in these arteries, it is important to acknowledge that these values, particularly SUV_{max}, may have been altered by spill-in effects from the adjacent coracosternal joints. Consequently, direct comparisons of SUV values between arteries might be limited, and the utility of PET scan measurements of arteries in close proximity to bony structures should be carefully considered.

While lesions were identified throughout the arteries on µPET scan, a tendency for increased ^{18}F-NaF uptake was notably observed at areas of bifurcation, such as the subclavian bifurcation of the brachiocephalic trunk and the celiac bifurcation of the abdominal aorta. The celiac localization of many aortic lesions was interesting because it is also the primary site of atherosclerotic lesions in the Carneau pigeon (*Columbia livia*) spontaneous model of this disease.[27] Atherosclerotic lesions in humans also commonly affect regions of bifurcation, suspected to be due to changes in blood flow and sheer stress at these sites.[28]

There was poor colocalization between lesions suspected on µPET scan and µCT scan. This was most apparent in the parrot that had a highly calcified lesion in the abdominal aorta on CT modalities but only mild ^{18}F-NaF uptake on µPET scan. Areas of microcalcification, as seen in earlier stages of atherosclerosis, have more hydroxyapatite surface area compared to later-stage macrocalcifications, where more of the hydroxyapatite molecules are contained within the center of the lesion. As a result, macroscopic calcium deposits have decreased ^{18}F-NaF uptake on PET scan and are better detected on CT scan. We suspect that the poor colocalization appreciated in our study is due to the differences in lesion types being detected by each modality as is seen in human medicine.[18] In addition, the poor colocalization for most lesions in this study was most likely attributed to lesion mischaracterization due to CBCT streak artifacts and increased noise.[26] These were more prominent in HAPs due to their smaller size and may reflect the higher detection frequency seen on µCT seen in this species compared to OWAPs.

A limitation of this study was that 2 different protocols were used for 2 different cohorts of Amazon parrots. Hispaniolan Amazon parrots are smaller than OWAPs, making the µCT scans of those birds more affected by image noise and streak artifacts. Higher SUV measurements were obtained for the OWAPs, which is likely due to the longer waiting period after injection of ^{18}F-NaF compared to the HAPs. We suspect that the longer waiting period led to more radiotracer uptake, resulting in more lesions being detected in this species, especially in the coronary arteries, which are harder to visualize due to nonspecific uptake in the blood pool of the cardiac chambers. This effect was somewhat mitigated in background corrected measurements. However, the OWAPs are also from an older population of birds, and so a true increased prevalence of atherosclerotic lesions cannot be ruled out. The longer waiting period used for the OWAPs also led to more ^{18}F-NaF pooling in the colon, which interfered with abdominal aorta assessment due to spill-in effects and resulted in overall higher background signal level. While increasing the waiting period was initially selected to decrease background activity, it led to the opposite effect and additional spill-in effects. Therefore, a waiting period of 1 hour is recommended after radiotracer administration based on these findings.

There are also inherent limitations to PET scanning for the detection of cardiovascular lesions. The effects of motion artifacts in particular may be exacerbated on PET scan images because the scanning time is longer than for CT scan and may alter some PET scan measurements.[29]

In conclusion, this study established a safe and effective protocol for ^{18}F-NaF molecular imaging of psittacine atherosclerosis for the first time. We demonstrated that µPET scan is a sensitive diagnostic tool for the detection of most clinically significant and some earlier stage atherosclerotic lesions in psittacines. While currently limited by availability and practicality, the application of ^{18}F-NaF PET scanning in psittacine bird vascular imaging has the potential to revolutionize the management of atherosclerosis in birds by enabling earlier and more accurate diagnosis. Further research is needed to optimize, standardize, and adapt scanning protocol to patients in hospital settings but also to further validate its diagnostic utility.

Acknowledgments

This study was funded by the Center for Companion Animal Health, School of Veterinary Medicine, University of California-Davis, and the Harrison Avian Research and Conservation Collaborative. The authors also thank Douglas J. Rowland, Charles M. Smith, Mariana Sosa Higareda, and Sarah M. Tam for their help acquiring diagnostic imaging of the parrots.

Disclosures

The authors have nothing to disclose. No AI-assisted technologies were used in the generation of this manuscript.

Funding

The authors have nothing to disclose.

ORCID

K. Brust https://orcid.org/0000-0001-9726-8879
M. Spriet https://orcid.org/0000-0001-9401-4857
H. Beaufrere https://orcid.org/0000-0002-3612-5548

Unauthenticated | Downloaded 04/19/25 06:02 AM UTC

References

1. Beaufrere H. Avian atherosclerosis: parrots and beyond. *J Exot Pet Med.* 2013;22(4):336–347. doi:10.1053/j.jepm.2013.10.015
2. Beaufrère H, Ammersbach M, Reavill DRDR, et al. Prevalence of and risk factors associated with atherosclerosis in psittacine birds. *J Am Vet Med Assoc.* 2013;242(12):1696–1704. doi:10.2460/javma.242.12.1696
3. Beaufrere H, Nevarez JG, Holder K, Pariaut R, Tully TN, Wakamatsu N. Characterization and classification of psittacine atherosclerotic lesions by histopathology, digital image analysis, transmission and scanning electron microscopy. *Avian Pathol.* 2011;40(5):531–544. doi:10.1080/03079457.2011.607427
4. Beaufrère H, Gardhouse SM, Wood RD, Stark KD. The plasma lipidome of the Quaker parrot (*Myiopsitta monachus*). *PLoS One.* 2020;15(4):e0240449. doi:10.1371/journal.pone.0240449
5. Beaufrère H, Nevarez JGG, Wakamatsu N, Clubb S, Cray C, Tully TN. Experimental diet-induced atherosclerosis in Quaker parrots (*Myiopsitta monachus*). *Vet Pathol.* 2013;50(6):1116–1126. doi:10.1177/0300985813488958
6. Beaufrere H, Stark KD, Wood RD. Effects of a 0.3% cholesterol diet and a 20% fat diet on plasma lipids and lipoproteins in Quaker parrots (*Myiopsitta monachus*). *Vet Clin Pathol.* 2022;51(3):376–384.
7. Pilny AA, Quesenberry KE, Bartick-Sedrish TE, Latimer KS, Berghaus RD. Evaluation of *Chlamydophila psittaci* infection and other risk factors for atherosclerosis in pet psittacine birds. *J Am Vet Med Assoc.* 2012;240(12):1474–1480. doi:10.2460/javma.240.12.1474
8. Beaufrère H. Blood lipid diagnostics in psittacine birds. *Vet Clin North Am Exot Anim Pract.* 2022;25(3):697–712. doi:10.1016/j.cvex.2022.05.003
9. Beaufrère H, Rodriguez D, Pariaut R, et al. Estimation of intrathoracic arterial diameter by means of computed tomographic angiography in Hispaniolan Amazon parrots. *Am J Vet Res.* 2011;72(2):210–218. doi:10.2460/ajvr.72.2.210
10. Yu PH, Lee YL, Chen CL, Chi CH. Comparison of three computed tomographic angiography protocols to assess diameters of major arteries in African grey parrots (*Psittacus erithacus*). *Am J Vet Res.* 2018;79(1):42–53. doi:10.2460/ajvr.79.1.42
11. Beaufrere H, Pariaut R, Rodriguez D, Tully TN. Avian vascular imaging: a review. *J Avian Med Surg.* 2010;24(3):174–184. doi:10.1647/2009-052.1
12. Aller TL, Guzman DS-M, Stern JA, et al. Evaluation of a fluoroscopic angiography protocol in Hispaniolan Amazon parrots (*Amazona ventralis*). *J Avian Med Surg.* 2022;36(2):178–186. doi:10.1647/21-00007
13. Lee YL, Yu PH, Chen CL, Wu YL, Chi CH. Determination of the enhancement effect and diameters of the major arteries of African grey parrots using a dual-head power injector for computed tomography angiography. *Taiwan Vet J.* 2015;41(3):165–175. doi:10.1142/S1682648515500134
14. Shioi A, Ikari Y. Plaque calcification during atherosclerosis progression and regression. *J Atheroscler Thromb.* 2018;25(4):294–303. doi:10.5551/jat.RV17020
15. Alexopoulos N, Raggi P. Calcification in atherosclerosis. *Nat Rev Cardiol.* 2009;6(11):681–688. doi:10.1038/nrcardio.2009.165
16. Nakahara T, Dweck MR, Narula N, Pisapia D, Narula J, Strauss HW. Coronary artery calcification: from mechanism to molecular imaging. *JACC Cardiovasc Imaging.* 2017;10(5):582–593. doi:10.1016/j.jcmg.2017.03.005
17. Sandfort V, Bluemke DA. CT calcium scoring. History, current status and outlook. *Diagn Interv Imaging.* 2017;98(1):3–10. doi:10.1016/j.diii.2016.06.007
18. Tzolos E, Dweck MR. 18F-sodium fluoride (18F-NaF) for imaging microcalcification activity in the cardiovascular system. *Arterioscler Thromb Vasc Biol.* 2020;40(7):1620–1626.
19. Irkle A, Vesey AT, Lewis DY, et al. Identifying active vascular microcalcification by 18F-sodium fluoride positron emission tomography. *Nat Commun.* 2015;6:7495. doi:10.1038/ncomms8495
20. Bassir A, Raynor WY, Park PSU, Werner TJ, Alavi A, Revheim ME. Molecular imaging in atherosclerosis. *Clin Transl Imaging.* 2022;10:259–272. doi:10.1007/s40336-022-00483-y
21. Gustavsen KA, Stanhope KL, Lin AS, Graham JL, Havel PJ, Paul-Murphy JR. Effects of exercise on the plasma lipid profile in Hispaniolan Amazon parrots (*Amazona ventralis*) with naturally occurring hypercholesterolemia. *J Zoo Wildl Med.* 2016;47(3):760–769. doi:10.1638/2015-0192.1
22. Fedorov A, Beichel R, Kalpathy-Cramer J, et al. 3D slicer as an image computing platform for the quantitative imaging network. *Magn Reson Imaging.* 2012;30(3):1323–1341. doi:10.1016/j.mri.2012.05.001
23. Akerele MI, Karakatsanis NA, Deidda D, et al. Comparison of correction techniques for the spillin effect in emission tomography. *IEEE Trans Radiat Plasma Med Sci.* 2020;4(4):422–432. doi:10.1109/TRPMS.2020.2980443
24. Yoon HC, Greaser LE, Mather R, Sinha S, McNitt-Gray MF, Goldin JG. Coronary artery calcium: alternate methods for accurate and reproducible quantitation. *Acad Radiol.* 1997;4(10):666–673. doi:10.1016/S1076-6332(97)80137-7
25. Ahuja K, Sotoudeh H, Galgano SJ, et al. 18F-sodium fluoride PET: history, technical feasibility, mechanism of action, normal biodistribution, and diagnostic performance in bone metastasis detection compared with other imaging modalities. *J Nucl Med Technol.* 2020;48(1):9–16. doi:10.2967/jnmt.119.234336
26. Schulze R, Heil U, Groβ D, et al. Artefacts in CBCT: a review. *Dentomaxillofacial Radiol.* 2011;40(5):265–273. doi:10.1259/dmfr/30642039
27. Anderson JL, Smith SC, Taylor RL. The pigeon (*Columba livia*) model of spontaneous atherosclerosis. *Poult Sci.* 2014;93(11):2691–2699. doi:10.3382/ps.2014-04280
28. Cunningham KS, Gotlieb AI. The role of shear stress in the pathogenesis of atherosclerosis. *Lab Invest.* 2005;85(1):9–23. doi:10.1038/labinvest.3700215
29. Mayer J, Wurster TH, Schaeffter T, et al. Imaging coronary plaques using 3D motion-compensated [18F]NaF PET/MR. *Eur J Nucl Med Mol Imaging.* 2021;48(8):2455–2465. doi:10.1007/s00259-020-05180-4

Unauthenticated | Downloaded 04/19/25 06:02 AM UTC